COMBINED NUMERICAL OPTIMIZATION AND CONSTRUCTAL THEORY FOR THE DESIGN OF MICRO-CHANNEL HEAT SINKS

by

Bello-Ochende T*., Meyer J.P., Ighalo F.U

*Author for correspondence

Department of Mechanical and Aeronautical Engineering,

University of Pretoria,

Pretoria, 0002,

South Africa,

E-mail: tbochende@up.ac.za

Abstract

This study deals with the geometric optimization of a silicon based micro-channel heat sink using a combined numerical optimization and constructal theory. The objective is to minimize the wall peak temperature subject to various constraints. The numerical simulations are carried out with fixed volumes ranging from 0.7 mm^3 to 0.9 mm^3 and pressure drop between 10 kPa to 60 kPa. The effect of pressure drop on the optimized aspect ratio, solid volume fraction, hydraulic diameter and the minimized peak temperature are reported. Results also show that as the dimensionless pressure drop increases the maximized global thermal conductance also increases.

Keywords: *Micro-channel, geometric optimization, thermal conductance, gradient based algorithm*

Nomenclature

A	[m^2]	Channel cross-sectional area
B	[m]	Channel width
Be	[-]	Bejan number
C	[-]	Global thermal conductance
C_p	[J/Kg]	Specific heat capacity
D	[m]	Diameter
$f(\boldsymbol{x})$	[-]	Objective function
$g_i(\boldsymbol{x})$	[-]	i-th equality constraint function
G	[m]	Computational domain width
$h_j(\boldsymbol{x})$	[m]	j-th equality constraint function
H	[m]	Computational domain height
k	[W/m.K]	Thermal conductivity
L	[m]	Channel axial length
Nu	[-]	Nusselt number
P	[Pa]	Pressure
$P[k]$	[-]	Successive sub-problem
q''	[W/m^2]	Heat flux
$\mathbb{R}^n$	[-]	n-dimensional real space
T	[K]	Temperature
t_1	[m]	Half thickness of vertical solid
t_2	[m]	Channel base thickness
t_3	[m]	Channel base to height distance
U	[m/s]	Velocity
V	[m^3]	Volume
W	[m]	Heat sink width
x,y,z	[m]	Cartesian coordinates

Greek symbols

α	[m^2/s]	Thermal diffusivity
Δ	[-]	Difference
μ	[kg/m.s]	Dynamic viscosity
ρ	[kg/m^3]	Density
ϕ	[-]	Volume fraction
∂	[-]	Step limit

Subscripts

c	Channel
f	Fluid
h	Hydraulic
max	Maximum
min	Minimum
opt	Optimum
s	Solid

Introduction

The impact of the new generation drive for high processing speed, sophisticated and compact electronic devices is the rising transistor density and switching speed of microprocessors. This challenge results in an increase in the amount of heat flux dissipation which is predicted to be in the excess of 100 W/cm^2 in the near future [1,2]. With this comes the need for advanced cooling techniques and micro-channels have recently generated great interest by researchers as it proves to yield high heat transfer rates.

As far back as 1981, Tuckerman and Pease [3] proposed that single phased microscopic heat exchangers using water as the coolant could achieve power density cooling of up to 1000 W/cm^2 and with experimentation; the cooling water could dissipate a heat flux of about 790 W/cm^2. Dirker and Meyer [4] developed correlations that predict the cooling performance of heat spreading layers in rectangular heat generating electronic modules. They discovered that the thermal performance was dependent on the geometric size of the volume posed by the presence of thermal resistance. Investigation into the heat transfer characteristics and fluid flow behaviour of micro-channels show that shape and geometric parameters such as the aspect ratio and hydraulic diameter of a micro-channel greatly influences the cooling capabilities of these heat sinks [5]. Wu and Cheng [6] showed experimentally that the friction factor of micro-channels may differ if their geometric configurations are different though their hydraulic diameters are the same. The trend of their experimental results showed an increase in the friction factor as the aspect ratio of the heat sink increased. Koo and Kleinstreuer [7] found out that the aspect ratio influences the viscous dissipation in micro-channels which in turn affects the heat transfer rate. Their work showed that as the aspect ratio deviated from unity, the dissipation effect increases. Chen [8] conducted an investigation into forced convection heat transfer within a micro-channel, it was reported that the heat transfer was influenced mainly by the aspect ratio and effective thermal conductivity of the heat sink. Muzychka [9] developed approximate expressions for the optimal geometry for various fundamental duct shapes. In his work, he showed

that the dimension of an optimal duct is independent of its array structure. Bello-Ochende *et al.* [10] presented a three dimensional geometric optimization of a micro-channel heat sink using scale analysis and intersection of asymptotes method. They used the constructal design theory to determine optimal geometric configurations that maximize the global thermal conductance in a dimensionless form. Ambatipudi and Rahman [11] numerically investigated the heat transfer within a micro-channel heat sink using silicon substrate. In their study, they explored the effects of channel depth and width across a range of Reynolds number. It was reported that at higher Reynolds number, higher heat transfer can be achieved. Their work also documented that optimum channel depth exists for various Reynolds number. Experimental and numerical techniques has been utilised to further investigate and maximize the cooling abilities of micro-channel heat sinks in recent researches [12-18]. In this work, an optimal geometry for a micro-channel heat sink is numerically determined which minimizes the peak wall temperature using mathematical optimization and constructal design theory.

Computational Model

Figure 1 shows the physical model and fig. 2 the computational domain for a micro-channel heat sink. The computational domain is an elemental volume selected from a complete micro-channel heat sink by the use of the symmetrical property of the heat sink. Heat is supplied to a highly conductive silicon substrate with known thermal conductivity from a heating area located at the bottom of the heat sink. The heat is then removed by a fluid flowing through a number of micro-channels. The heat transfer in the elemental volume is a conjugate problem that combines heat conduction in the solid and convective heat transfer in the liquid.

Figure 3 shows the computational domain and its grid sizes. The following assumptions were made to model the heat transfer and fluid flow in the elemental volume:

- The hydraulic diameter of the micro-channel under analysis is greater than 10 μm
- For water, the continuum regime applies hence the Navier-Stokes and Fourier equations can still be used to describe the transport processes
- Steady-state conditions for flow and heat transfer
- Incompressible flow
- Constant solid and fluid properties
- Negligible heat transfer due to radiation and natural convection
- Negligible buoyancy and viscous heating
- Large number of micro-channels

Based on the assumptions listed above, the continuity, momentum and energy equations governing the fluid flow and heat transfer for the cooling fluid within the heat sink are given in eqs. (1), (2) and (3) respectively.

$$\nabla(\rho \boldsymbol{U}) = 0 \tag{1}$$

$$\rho(\boldsymbol{U}.\nabla \boldsymbol{U}) + \Delta P - \mu \nabla^2 \boldsymbol{U} = 0 \tag{2}$$

$$\rho C_{\mathrm{p}}(\boldsymbol{U}.\nabla T) - k_{\mathrm{f}} \nabla^2 T = 0 \tag{3}$$

For the solid material, the momentum and energy governing equations are given by eq. (4) and eq. (5) below.

$$\boldsymbol{U} = 0 \tag{4}$$

$$k_{\mathrm{s}} \nabla^2 T = 0 \tag{5}$$

The conjugate heat transfer problem is modelled with heat being supplied to the bottom wall of the heat sink at 1 MW/m^2. Water at 20°C is pumped through the channel across the axial length with a pressure drop ranging between 10 kPa and 60 kPa. A vertex-centred finite volume code was used to solve the continuity, momentum and energy equations using the appropriate boundary conditions. A second order upwind scheme was used in discretizing the momentum equation while a SIMPLE algorithm was used for the pressure-velocity coupling. Convergence criteria was set to less than $1\text{x}10^{-4}$ for continuity and momentum residuals while the residual of energy was set to less than $1\text{x}10^{-7}$.

Code Validation

To ensure accuracy of the results, mesh refinement was performed until a mesh size with negligible changes in thermal resistance was obtained. The grid dependence test was conducted using five different mesh sizes having 19 200, 25 920, 57 600, 88 000 and 110 880 grid cells. The computational volume whose dimensions are given in table 1 was used for the analysis. From the results given in table 2a and table 2b (for inlet pressures of 30 kPa and 60 kPa respectively), it follows that a mesh of 57 600 cells assures a less than 1% change in the thermal resistance with increasing mesh size. Thus a mesh with 57 600 cells was chosen for the numerical simulation as it will guarantee results which are independent of mesh size.

The numerical code was then evaluated by comparing the results generated with available widely accepted analytical results. Figures 4 and 5 show the numerical and analytical dimensionless velocity profile for fully developed flow within the micro-channel along the x and y axis respectively. The velocity profile for the numerical solution was generated at the centre of the channel. Shah and London [19] analytical solution was used to compare with the numerical prediction obtained and an excellent agreement was found.

The energy equation was also verified by comparing the pure convective Nusselt number Nu to that given by Shah and London [19] with this comparison shown in figure 6. Using a constant longitudinal wall heat flux with uniform peripheral heat flux boundary condition, a high Nu is experienced at the entrance region but converges to the analytical Nu once fully developed.

Numerical Optimization

The geometric optimization of the conjugate heat transfer problem was solved using a robust gradient based optimization algorithm which does not require an explicit line search. The DYNAMIC-Q optimization algorithm applies the dynamic trajectory LFOPC optimization algorithm to successive quadratic approximations of the actual optimization problem [20]. This algorithm was found to offer equal competitiveness when compared to the sequential quadratic programming (SQP) method [21] and was proved to be superior to SQP when handling optimization problem with severe noise [22]. Consider a typical constrained optimization problem of the form:

$$\begin{aligned} &\underset{\text{with respect to x}}{\text{minimize}}\ \mathrm{f}(\boldsymbol{x}),\ \ \boldsymbol{x}=[x_1,x_2,..x_l..,x_n]^T, x_l \in \mathbb{R}^n \\ &\text{subject to the constraints:} \\ &\mathrm{g}_i(\boldsymbol{x}) \le 0,\ \ i=1,2,...,m \\ &\mathrm{h}_j(\boldsymbol{x}) = 0,\ \ j=1,2,...,r \end{aligned} \tag{6}$$

In this method, successive sub-problems $\mathrm{P}[k],\ k=0,1,2,...$ are generated at successive design points $\boldsymbol{x}^k$ by constructing spherically quadratic approximations which are used to approximate the objective functions or constraints (or both) if they are not analytically given or very expensive to compute numerically [21,13]. These spherical quadratic approximations are given by eq. (7).

$$\begin{aligned} \tilde{\mathrm{f}}(\boldsymbol{x}) &= \mathrm{f}(\boldsymbol{x}^k) + \nabla^T \mathrm{f}(\boldsymbol{x}^k)(\boldsymbol{x}-\boldsymbol{x}^k) + \frac{1}{2}(\boldsymbol{x}-\boldsymbol{x}^k)\mathbf{A}(\boldsymbol{x}-\boldsymbol{x}^k) \\ \tilde{\mathrm{g}}_i(\boldsymbol{x}) &= \mathrm{g}_i(\boldsymbol{x}^k) + \nabla^T \mathrm{g}_i(\boldsymbol{x}^k)(\boldsymbol{x}-\boldsymbol{x}^k) + \frac{1}{2}(\boldsymbol{x}-\boldsymbol{x}^k)\mathbf{B}_i(\boldsymbol{x}-\boldsymbol{x}^k) \\ \tilde{\mathrm{h}}_j(\boldsymbol{x}) &= \mathrm{h}_j(\boldsymbol{x}^k) + \nabla^T \mathrm{h}_j(\boldsymbol{x}^k)(\boldsymbol{x}-\boldsymbol{x}^k) + \frac{1}{2}(\boldsymbol{x}-\boldsymbol{x}^k)\mathbf{C}_j(\boldsymbol{x}-\boldsymbol{x}^k) \end{aligned} \tag{7}$$

$\boldsymbol{A}$, $\boldsymbol{B}_i$ and $\boldsymbol{C}_j$ are the Hessian matrices of the objective, inequality and equality functions respectively. The gradient vector of the objective function $\nabla^T \mathrm{f}$ with respect to each design variable x_l is approximated by a first-order finite difference scheme.

$$\frac{\partial \mathrm{f}(\boldsymbol{x})}{\partial x_l} = \frac{\mathrm{f}(\boldsymbol{x} + \Delta \boldsymbol{x}_l) - \mathrm{f}(\boldsymbol{x})}{\Delta \boldsymbol{x}_l} \quad \forall\ l = 1, 2, ..., n \tag{8}$$

with $\Delta \boldsymbol{x}_l \quad [0, 0, ..., \Delta x_l, ...0]^T$ being an appropriate differencing step size. On the other hand, the gradient vectors for the equality $\nabla^T \mathrm{h}_j$ and inequality $\nabla^T \mathrm{g}_i$ functions which are required at each design point and for the construction of successive sub-problems are provided analytically.

Move limits δ_l are used to ensure convergence in a stable and controlled manner and are implemented in the form of an additional constraint.

$$\begin{aligned} &\boldsymbol{x}_l - \boldsymbol{x}_l^k - \delta_l \le 0 \\ &-\boldsymbol{x}_l + \boldsymbol{x}_l^k - \delta_l \le 0 \\ &\text{with } l = 1, 2, ..., n \end{aligned} \tag{9}$$

The DYNAMIC-Q algorithm terminates when the norm of the step size or function value is less than a specified tolerance.

Problem Formulation

It is required to determine the best geometric configuration of a micro-channel heat sink that will provide an optimal peak wall temperature and in turn maximize the global thermal conductance of the heat sink subject to various constraints. This optimal value is achieved by the relaxation of the geometric parameters t_1, t_2, t_3, H and G for the fixed axial length case and an additional variable L as depicted in fig. 1 for the variable length case.

Constraints

- Solid Volume Fraction: The solid volume fraction ϕ which is defined as the ratio of solid volume material to the total volume of the micro-channel heat sink is allowed to vary between 0.3 and 0.8.

$$0.3 \le \left[\phi = \frac{V_s}{V} = \frac{A_s L}{AL} \quad \frac{A_s}{A} \right] \le 0.8 \tag{10}$$

- Manufacturing Restraints: Assuming the DRIE manufacturing technique [24,25] was employed in the fabrication of the heat sink, the maximum allowable aspect ratio is 20. Also the minimum allowable thickness of the top and bottom wall is 50 μm [26,27].

- Total Fixed Volume: For each optimization problem, the computational volume is kept constant.

Optimization Process

The optimization problem is solved without any human intervention. This automated process is achieved by coupling the DYNAMIC-Q algorithm with computational fluid dynamics (FLUENT [28]) and grid generation (GAMBIT [29]) code in a MATLAB [30] environment. Figure 7 shows the flow diagram of the optimization process which is carried out until convergence by either the step size or function value criteria are reached. A multi starting guess approach is used to ensure the converged solution is indeed the global minimum with sensitivity analysis conducted to decide upon the appropriate differencing step size to implement on the forward differencing scheme.

Results

The optimization process when applied to a constant computational volume of 0.9 mm^3 with pressure drop varying from 10 kPa to 60 kPa, five geometric parameters are varied to obtain an optimal maximum wall temperature of the micro-channel subject to the formulated constraints.

Figure 8 shows the relationship between the minimised peak wall temperatures of a micro-channel for a range of pressure drop. It can be seen that the minimised peak wall temperature decreases with increasing pressure drop because as the velocity increases, the thermal resistance decreases. This non-linear trend is in agreement with already published work in open literature [10, 26, 31]. This relationship between pressure drop and the optimal peak wall temperature difference suggests that with a higher pressure drop, improved cooling capabilities can be achieved; however, due to the rising cost that is associated with pumping power, a trade-off will be vital in order to achieve the optimal benefit from such systems.

Figure 9 shows the effect of pressure drop on the optimal solid volume fraction ϕ_{opt}. As the pressure drop increases ϕ_{opt} also increases. An approximate linear relationship exist between ϕ_{opt} and the pressure drop. Figure 9 also shows that the optimal solid volume fraction ranges between 0.3 and 0.5 which agrees with the results published by Bello-Ochende *et al.* [10]. As shown in fig. 10, the optimal aspect ratio of the micro-channel exhibits varying relationship in relation to a change in the applied pressure drop. With an increase in pressure drop, an increase in the optimal aspect ratio is observed up until 35 kPa. There is a decrease in the aspect ratio with any further increase in pressure drop.

A decrease in the optimal hydraulic diameter (fig. 11a) of the heat sink is also observed with an increase in the pressure drop applied across the channel. This decrease continues until it is such that the cooling fluid is been "squeezed" into the channel. Further increase in the pressure drop causes the optimal hydraulic diameter to increase in order to ensure the flow is not overworked. Bello-

Ochende *et al.* [10] derived an analytical expression which approximates the optimal hydraulic diameter of a cooling channel with heat flux supplied at the base to be

$$D_{h,opt} \approx 1.86\left(L^3V\right)^{1/6} Po^{3/8} Be^{-1/4} \tag{11}$$

with the Poiseuille number approximated as

$$Po = \frac{12}{\left(1+\frac{B}{H_c}\right)^2\left[1-\frac{192}{\pi^5}\frac{B}{H_c}\tanh\left(\frac{\pi}{2}\frac{H_c}{B}\right)\right]} \tag{12}$$

The numerical result of the optimal hydraulic diameter compares well with this theoretical approximation with deviations of less than 10% found as shown in figure 11b. The optimal hydraulic diameter ranges from 120 μm to 140 μm and this validates the assumption made when defining our computational model. Figure 12 shows the relationship between the maximised global thermal conductance as a function of Bejan number. The global thermal conductance C is a dimensionless ratio of the heat transfer rate to the peak wall temperature difference of a heat sink and it is expressed as

$$C = \frac{q"L}{k\left(\Delta T_{\max}\right)} \tag{13}$$

The dimensionless pressure drop (Bejan number) is also expressed as

$$\mathrm{Be} = \frac{\Delta P V^{2/3}}{\alpha\mu} \tag{14}$$

It is demonstrated that the maximised global thermal conductance increases linearly with an increase in the dimensionless pressure drop. Bello-Ochende *et al.* [10] predicted using theoretical analysis that the maximum thermal conductance is $C_{\max,\mathrm{theory}} = 0.6Be^{0.49}$ for micro-channel with uniform hear flux at its base. Figure 12 also shows similar trends when comparing the maximized global thermal conductance with the theoretical and numerical prediction of Bello-Ochende *et al.* [10].

The volume constraint was relaxed and then decreased gradually from the initial set volume of 0.9 mm^3 to investigate the influence of the computational volume on the heat sink optimal dimensions. Table 2 gives the design results for a range of constant computational volume $0.7\ \mathrm{mm}^3 \le V \le 0.9\ \mathrm{mm}^3$ when a pressure drop of 50kPa is applied across the micro-channel. These results show a decrease in the minimized wall peak temperature with an increase in the heat sink volume as the heat generated within the volume increases as the heat sink volume is decreased. The table also shows that the optimized volume fraction ϕ_{opt} and hydraulic diameter increases as the volume increases.

The optimization process was then executed with the length not fixed to 10 mm but relaxed. This increases the degrees of freedom of the heat sink thereby obtaining an optimal length. It proved

to offer better optimal cooling effects (fig. 13) at lower pressure drops with a more than 16% decrease in the optimal peak wall temperature difference at 10 kPa.

Table 3 gives the optimal design parameters for the heat sink when the axial length is relaxed. The results show a linear increasing trend of the optimized aspect ratio as a function of the applied pressure drop with the ratio of solid volume to total volume between 0.4 and 0.45. This optimal configuration provides improved heat transfer capabilities with an increased maximized global thermal conductance of the heat sink of up to 20% at low pressures.

Figure 14 depicts a linear relationship between the optimized length and the applied pressure drop. The result shows that as the pressure drop is increased, the resulting optimal channel configuration will be of a longer but slender nature.

Figure 15(a) shows the temperature contour of the heat sink across the length of the heat sink. It shows the gradual increase in temperature along its length with the bottom wall experiencing the greater amount of heat. Figure 15(b) gives the temperature distribution of the heat sink along the transverse axis showing an increase in temperature from the channel top wall to the hot spot bottom wall.

Conclusion

In this paper, it has been demonstrated that numerical simulations and mathematical optimization can be used to optimally design micro-channels. For a pressure drop range between 10 kPa and 60 kPa, the optimal peak wall temperature decreased exponentially with an increase in pressure. It has been shown that a unique optimal geometric configuration exists for a given pressure drop applied across a channel that will result in a minimized peak wall temperature. Furthermore, taking more design parameters into account will result in even better cooling capabilities of micro-channel heat sinks as up to 20% increase in the global thermal conductance were obtained when the axial length was relaxed in the optimization process.

Acknowledgments

This work was supported by the Advanced Engineering Centre of Excellence at the University of Pretoria, National Research Foundation (NRF) of South Africa, TESP, EEDSM Hub and the CSIR.

References

1. F. J. Hong, P. Cheng, H. Ge, T. J. Goh, Conjugate heat transfer in fractal-shaped microchannel network heat sink for integrated micoelectronic cooling application, Int. J. Heat Mass Transfer, vol. 50, pp. 4986-4998, 2007.
2. K. C. Toh, X. Y. Chen, J. C. Chai, Numerical computation of fluid flow and heat transfer in microchannels, Int. J. Heat Mass Transfer, vol. 45, pp. 5133-5141, 2002.
3. D. B. Tuckerman, R. F. W. Pease, High performance heat sinking for VLSI, IEE Electron Device Letters, vol. 2, pp. 126-129, 1981.
4. J. Dirker, J. P. Meyer, Thermal characterisation of embedded heat spreading layers in rectangular heat-generating electronic modules, Int. J. Heat Mass Transfer, vol. 52, pp. 1374-1384, 2009.
5. H. Y. Wu, P. Cheng, An experimental study of convective heat transfer in silicon microchannels with different surface conditions, Int. J. Heat Mass Transfer, vol. 46, pp. 2547–2556, 2003.
6. H. Y. Wu, P. Cheng, Friction factors in smooth trapezoidal silicon microchannels with different aspect ratios, Int. J. Heat Mass Transfer, vol. 46, pp. 2519–2525, 2003.
7. J. Koo, C. Kleinstreuer, Viscous dissipation effects in microtubes and microchannels, Int. J. Heat Mass Transfer, vol. 47, pp. 3159–3169, 2004.
8. C. Chen, Forced convection heat transfer in microchannel heat sinks, Int. J. Heat Mass Transfer, vol. 50, pp. 2182–2189, 2007.
9. Y. S. Muzychka, Constructal design of forced convection cooled microchannel heat sinks and heat exchangers, Int. J. Heat Mass Transfer, vol. 48, pp. 3119–3127, 2005.
10. T. Bello-Ochende, L. Liebenberg, J. P. Meyer, Constructal cooling channels for micro-channel heat sinks, Int. J. Heat Mass Transfer, vol. 50, pp. 4141-4150, 2007.
11. K. K. Ambatipidi, M. M. Rahman, Analysis of conjugate heat transfer in mircochannel heat sinks, Numerical Heat Transfer, Part A: Applications, vol. 37, no. 7, pp. 711-731, 2000.
12. G. Gamrat, M. Favre-Marinet, D. Asendrych, Conduction and entrance effects on laminar liquid flow and heat transfer in rectangular microchannels, Int. J. Heat Mass Transfer, vol. 48, pp. 2943–2954, 2005.

13. Z. Guo, Z. Li, Size effects on single-phase channel flow and heat transfer at microscale, Int. J. Heat Fluid Flow, vol. 24, pp. 284–298, 2003.
14. W. Qu, I. Mudawar, Analysis of three-dimensional heat transfer in micro-channel heat sinks, Int. J. Heat Mass Transfer, vol. 45, pp. 3973–3985, 2002.
15. Z. Sun, Y. Jaluria, Unsteady two-dimensional nitrogen flow in long microchannels with uniform wall heat flux, Numerical Heat Transfer, Part A: Applications, vol. 57, no. 9, pp. 625-641, 2010.
16. Z. C. Hong, C. E. Zhen, C. Y. Yang, Fluid dynamics and heat transfer analysis of three dimensional microchannel flow with microstructures, Numerical Heat Transfer, Part A: Applications, vol. 54, no. 3, pp. 293-314, 2008.
17. E. Y. K. Ng, S. T. Poh, CFD analysis of double-layer microchannel conjugate parallel liquid flows with electric double-layer effects, Numerical Heat Transfer, Part A: Applications, vol. 40, no. 7, pp. 735-749, 2001.
18. C. S. Chen, Numerical analysis of gas flow in microchannels, Numerical Heat Transfer, Part A: Applications, vol. 33, no. 7, pp. 749-762, 1998.
19. R. K. Shah, A. L. London, Laminar Flow Forced Convection in Ducts: a Source Book for Compact Heat Exchanger Analytical Data, Supl. 1. Academic Press, New York, 1978.
20. J. A. Snyman, Practical Mathematical Optimization: An Introduction to Basic Optimization Theory and Classical and New Gradient-Based Algorithms, Springer, New York, 2005.
21. J. A. Snyman, A. M. Hay, The DYNAMIC-Q Optimization Method: An Alternative to SQP?, Computer and Mathematics with Applications, vol. 44, pp. 1589-1598, 2002.
22. P. S. Els, P. E. Uys, Investigation of the applicability of the Dynamic-Q optimisation algorithm to vehicle suspension design, Mathematical and Computer Modelling, vol. 37, pp. 1029-1046, 2003.
23. D. J. De Kock, Optimal Tundish Methodology in a Continuous Casting Process. PhD Thesis, Department of Mechanical and Aeronautical Engineering, University of Pretoria, 2005.
24. F. Laermer, A. Urban, Challenges, developments and application of silicon deep reactive ion etching, Microelectronic Engineering, vol. 67-68, pp. 349-355, 2003.
25. M. J. Madou, “MEMS Fabrication,” in MEMS Handbook, M. Gad-el-Hak, Ed., Boca Raton, FL: CRC, 2002.

26. A. Husain, K. Kim, Shape Optimization of Micro-Channel Heat Sink for Micro-Electronic Cooling, IEEE Transactions on Components and Packaging Technologies, vol. 31, no. 2, pp. 322-330, 2008.
27. J. Li, G. P. Peterson, Geometric Optimization of a Micro Heat Sink with Liquid Flow, IEEE Transactions on Components and Packaging Technologies, vol. 29, no. 1, pp. 145-154, 2006.
28. Fluent Inc., Fluent Version 6 Manuals, Centerra Resource Park, 10 Cavendish Court, Lebanon, New Hampshire, USA, 2001, http://www.fluent.com/
29. Fluent Inc., Gambit Version 6 Manuals, Centerra Resource Park, 10 Cavendish Court, Lebanon, New Hampshire, USA, 2001, http://www.fluent.com/
30. The MathWorks, Inc., MATLAB & Simulink Release Notes for R2008a, 3 Apple Hill Drive, Natick, MA, 2008, http://www.mathworks.com/
31. A. Husain, K. Kim, Multiobjective Optimization of a Microchannel Heat Sink using Evolutionary Algorithm, J. Heat Transfer, vol. 130, pp. 1-3, 2008.

Table 1. Dimensions of Micro-channel Heat Sink for Code Validation

t_1 (mm)	t_2 (mm)	t_3 (mm)	B (mm)	H_c (mm)	G (mm)	H (mm)	L (mm)
0.02	0.21	0.69	0.06	0.48	0.1	0.9	10

Table 2a. Grid Independence Test Results at 30 kPa

Number of Cells	Thermal Resistance ($K.cm^3/W$)	Difference
19 200	0.118	-
25 920	0.118	0.14%
57 600	0.122	1.33%
88 000	0.125	0.73%
110 880	0.126	0.29%

Table 2b. Grid Independence Test Results at 60 kPa

Number of Cells	Thermal Resistance ($K.cm^3/W$)	Difference
19 200	0.0879	-
25 920	0.0881	0.09%
57 600	0.0916	1.20%
88 000	0.0920	0.16%
110 880	0.0924	0.13%

Table 3. Optimal design results for various computational volumes

Volume (mm^3)	Minimized Peak Temperature (^oC)	Optimized Aspect Ratio $(H_c/B)_{opt}$	Optimized Volume Fraction ϕ_{opt}	(D_h)opt (mm)
0.9	29.53	11.752	0.425	0.122
0.8	29.79	10.069	0.425	0.123
0.7	30.12	10.359	0.386	0.118

Table 4. Optimal design results when the axial length is relaxed

Pressure Drop (kPa)	Optimised Aspect Ratio $(H_c/B)_{opt}$	Optimised Volume Fraction ϕ_{opt}	$(D_h)_{opt}$ (mm)	C_{max}
60	11.831	0.440	0.126	1 884.3
50	11.341	0.439	0.131	1 790.6
40	10.753	0.440	0.139	1 683.5
30	10.079	0.429	0.149	1 543.5
20	9.170	0.407	0.161	1 354.9
10	7.873	0.382	0.188	1 081.8

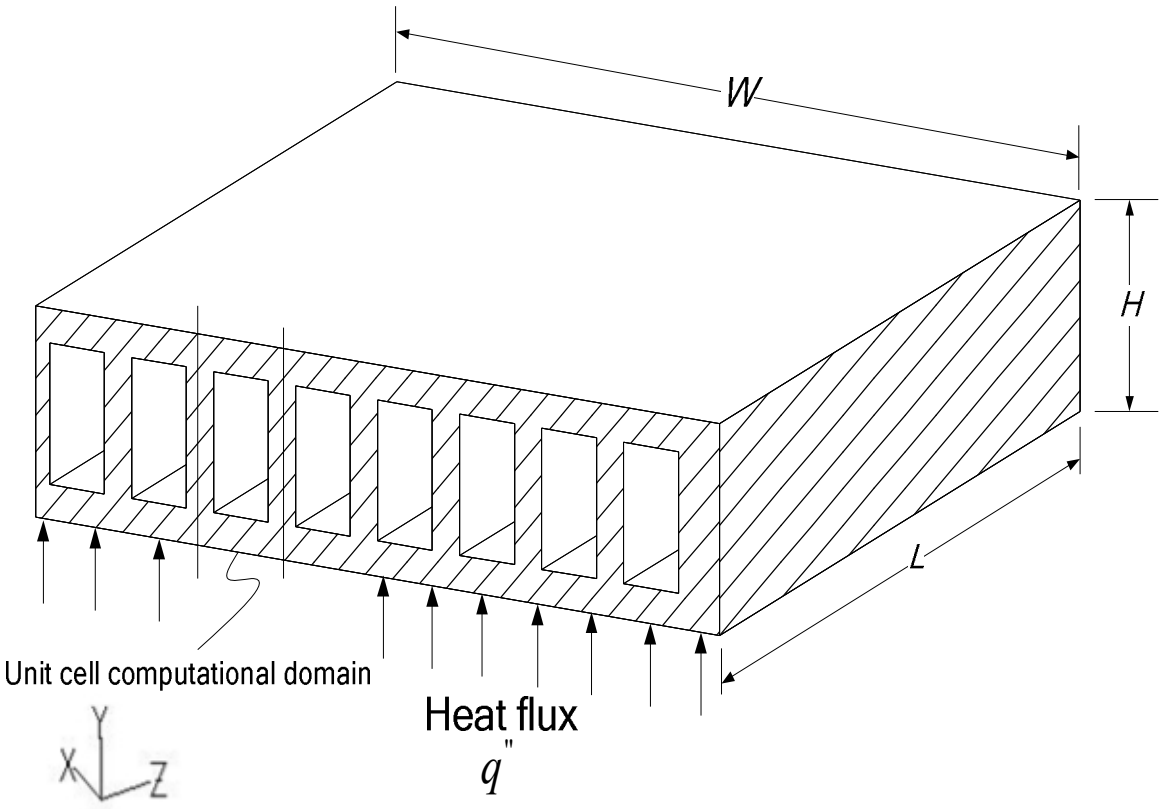

Figure 1. Physical model of a micro-channel heat sink

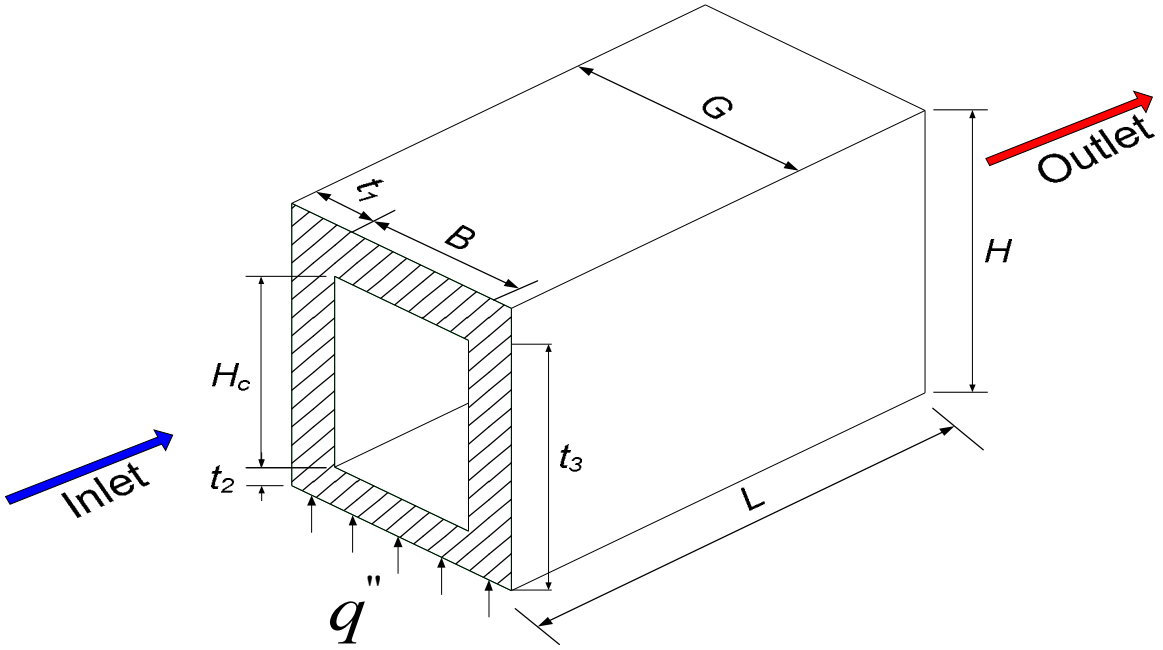

Figure 2. Unit cell computational domain for a micro-channel heat sink

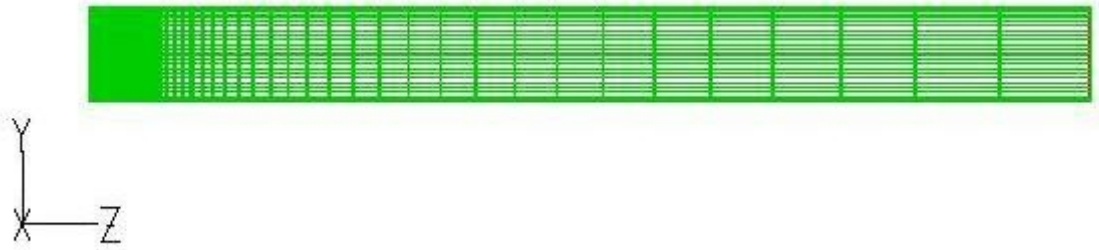

Figure 3a. Mesh grid (across the longitudinal axis) generated for numerical computation

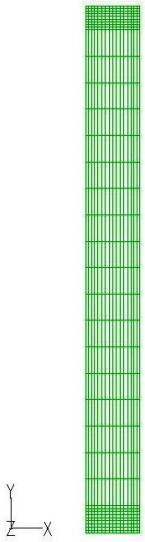

Figure 3b. Mesh grid (across the transverse axis) generated for numerical computation

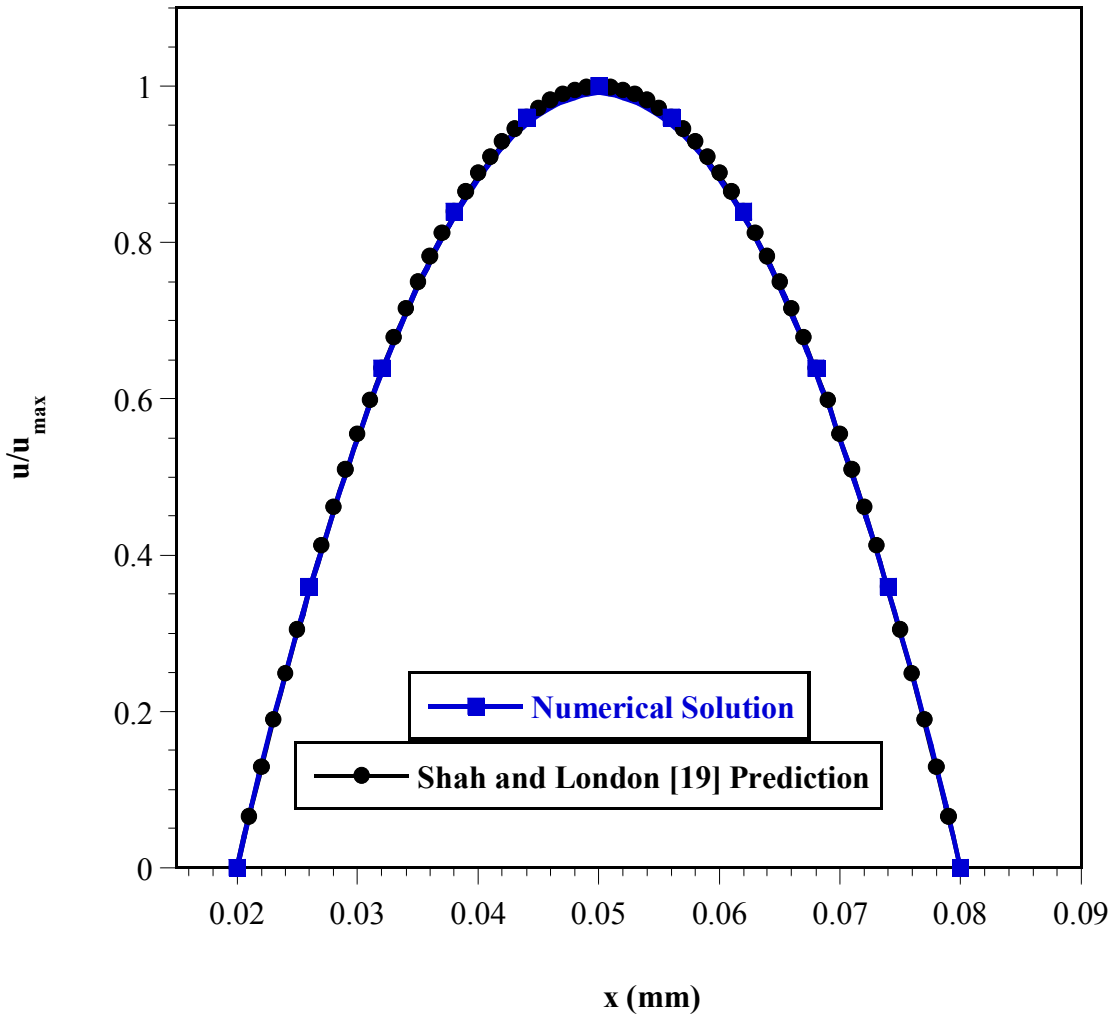

Figure 4. Comparison between numerical and analytical prediction for fully developed velocity profile along the x-axis

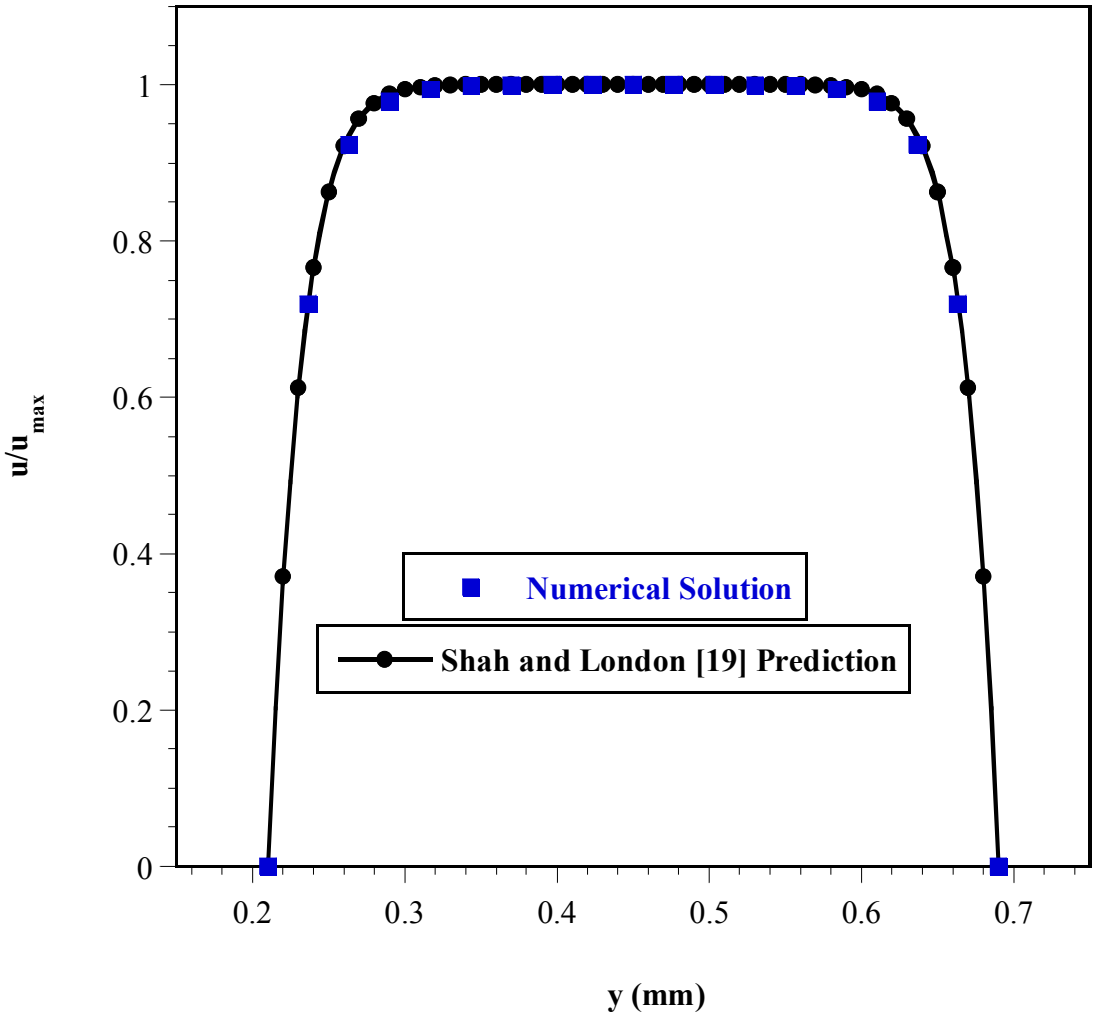

Figure 5. Comparison between numerical and analytical prediction for fully developed velocity profile along the y-axis

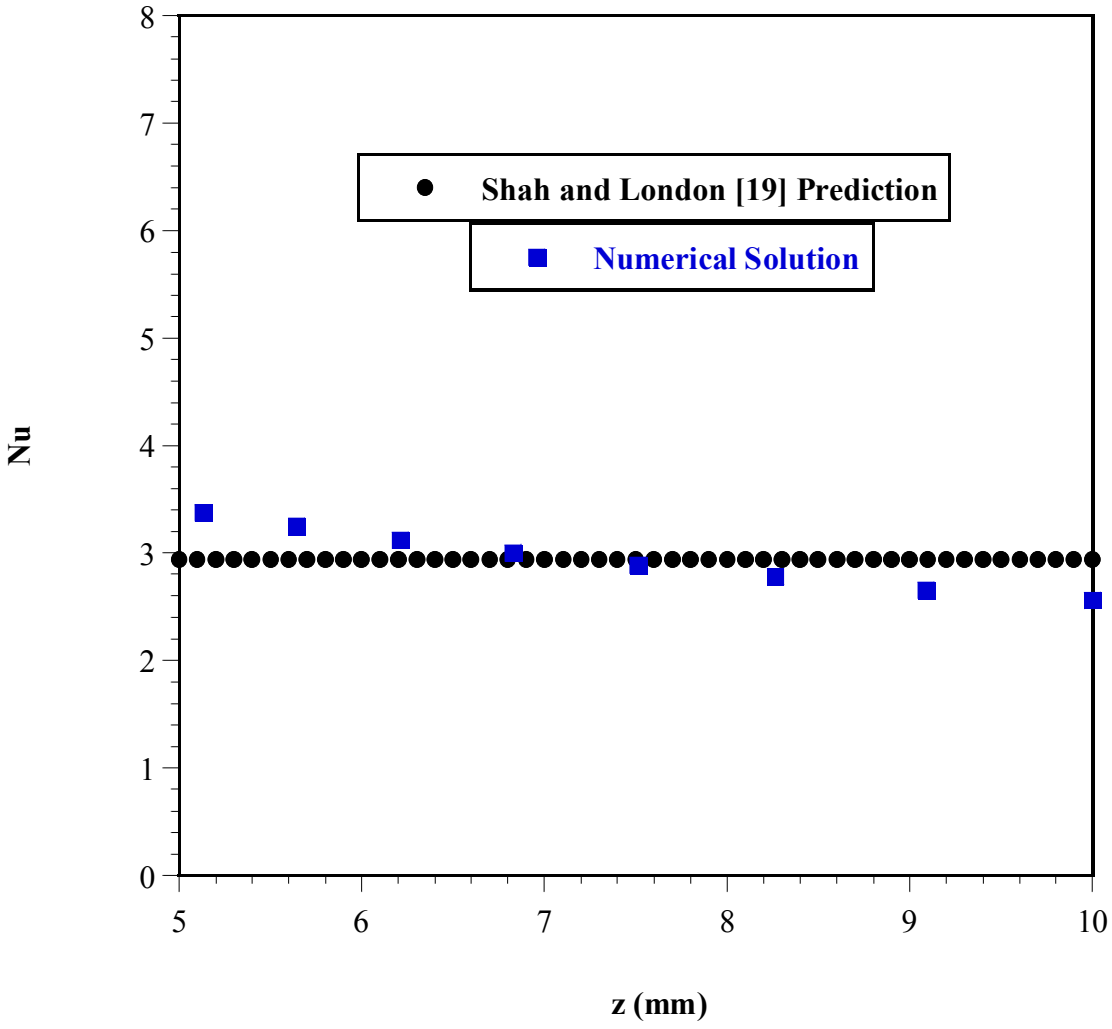

Figure 6. Comparison between numerical and analytical prediction for Nu profile along the channel length

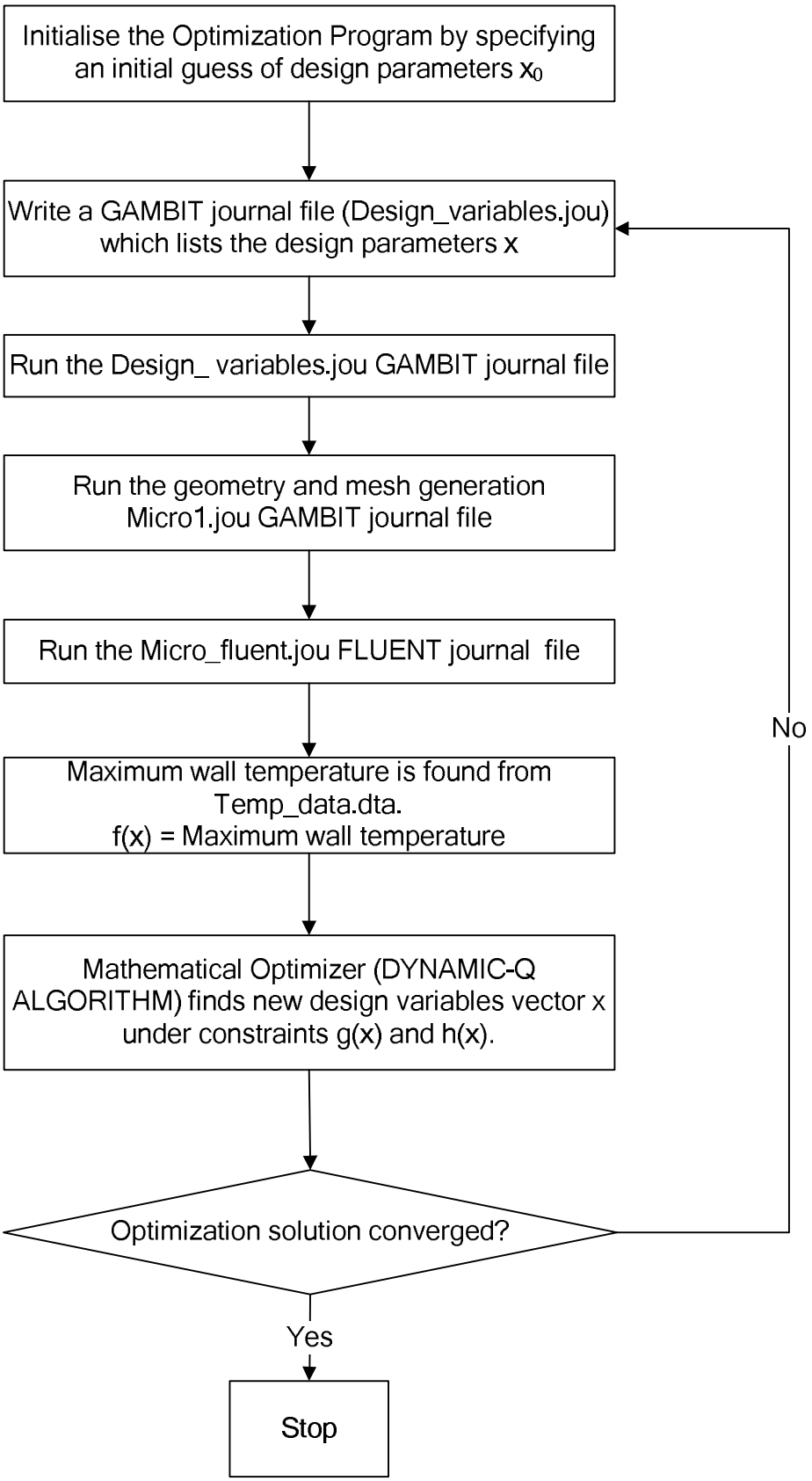

Figure 7. The optimization process flow chart

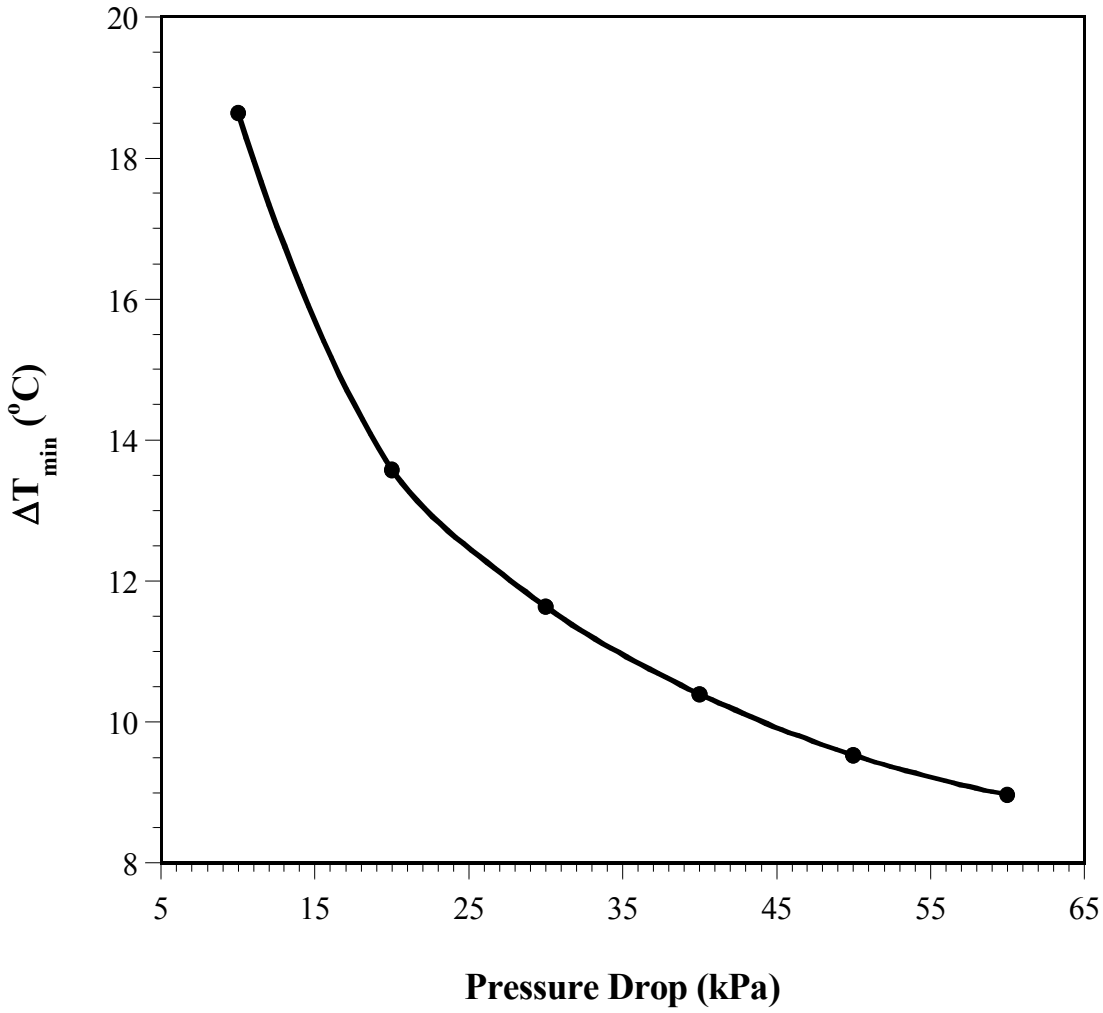

Figure 8. The influence of pressure drop on the optimal peak wall temperature difference

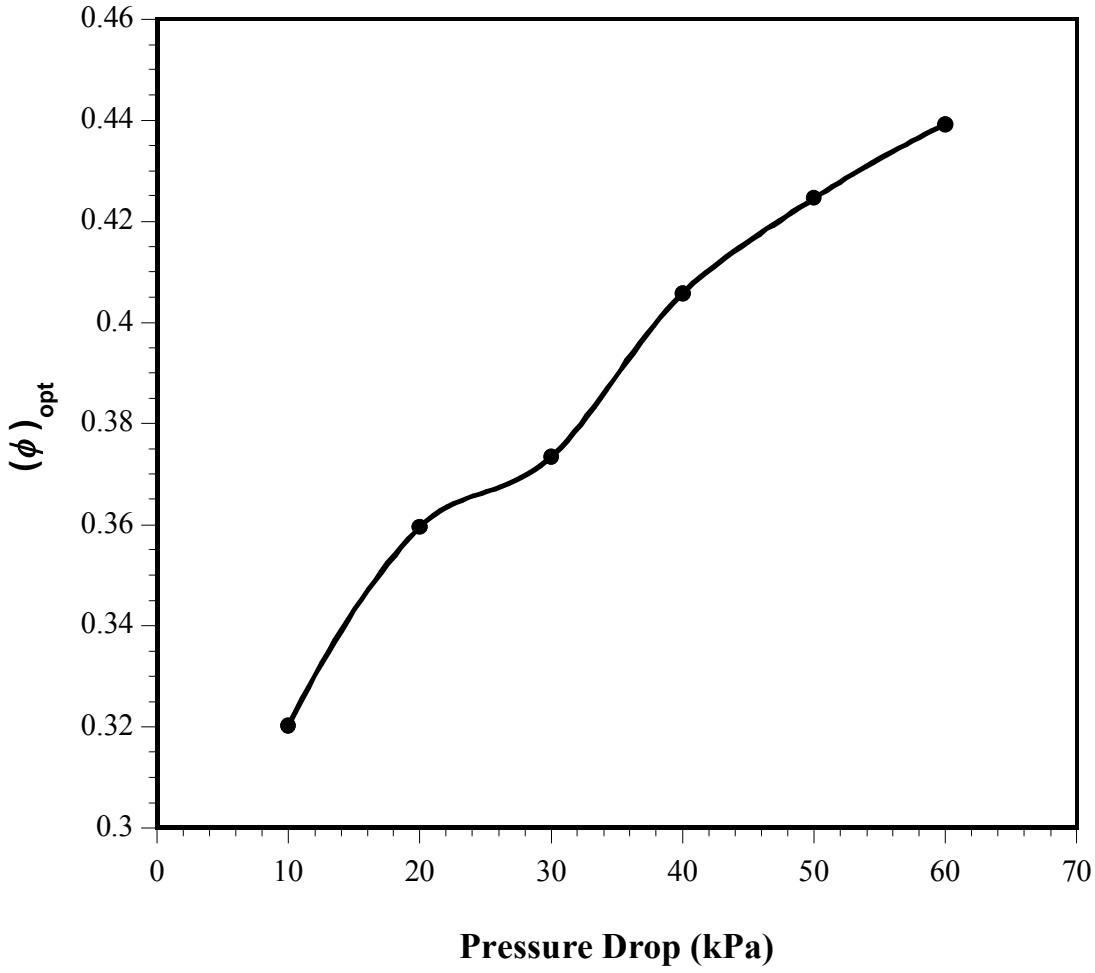

Figure 9. The effect of the change in pressure drop on the optimal solid volume fraction

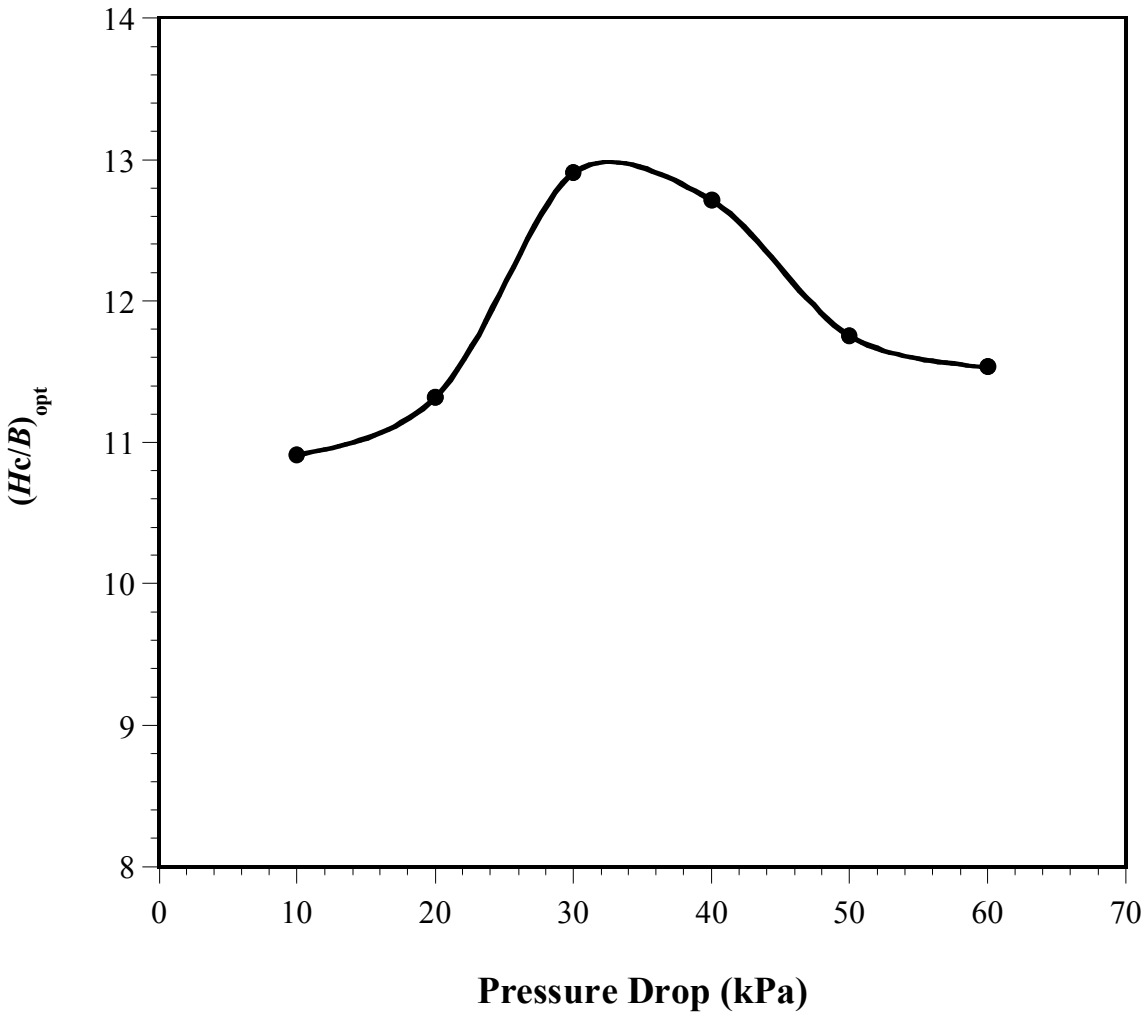

Figure 10. The effect of the change in pressure drop on the optimal channel aspect ratio

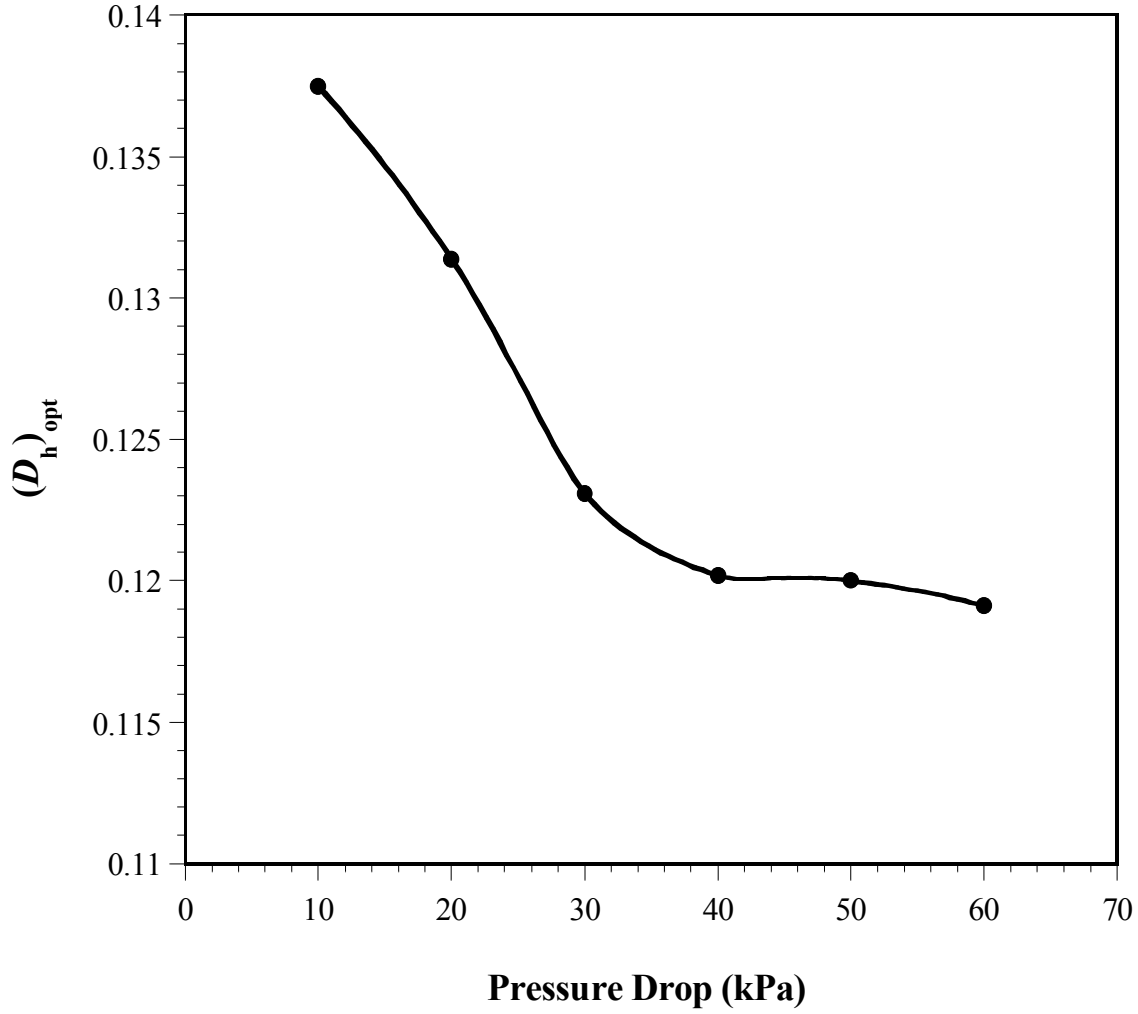

Figure 11a. The effect of the change in the pressure drop parameter on the optimal hydraulic diameter

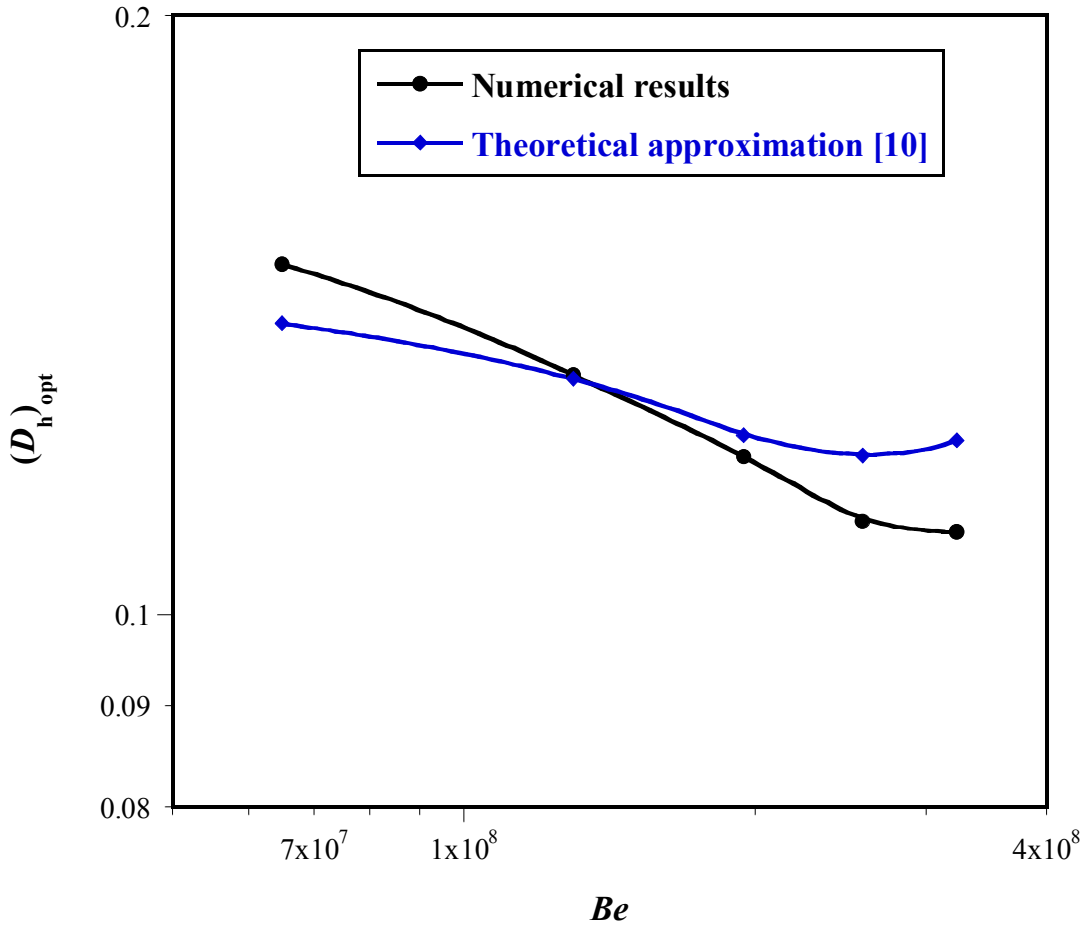

Figure 11b. Numerical and theoretical comparison of the optimal hydraulic diameter as a function of the dimensionless pressure drop

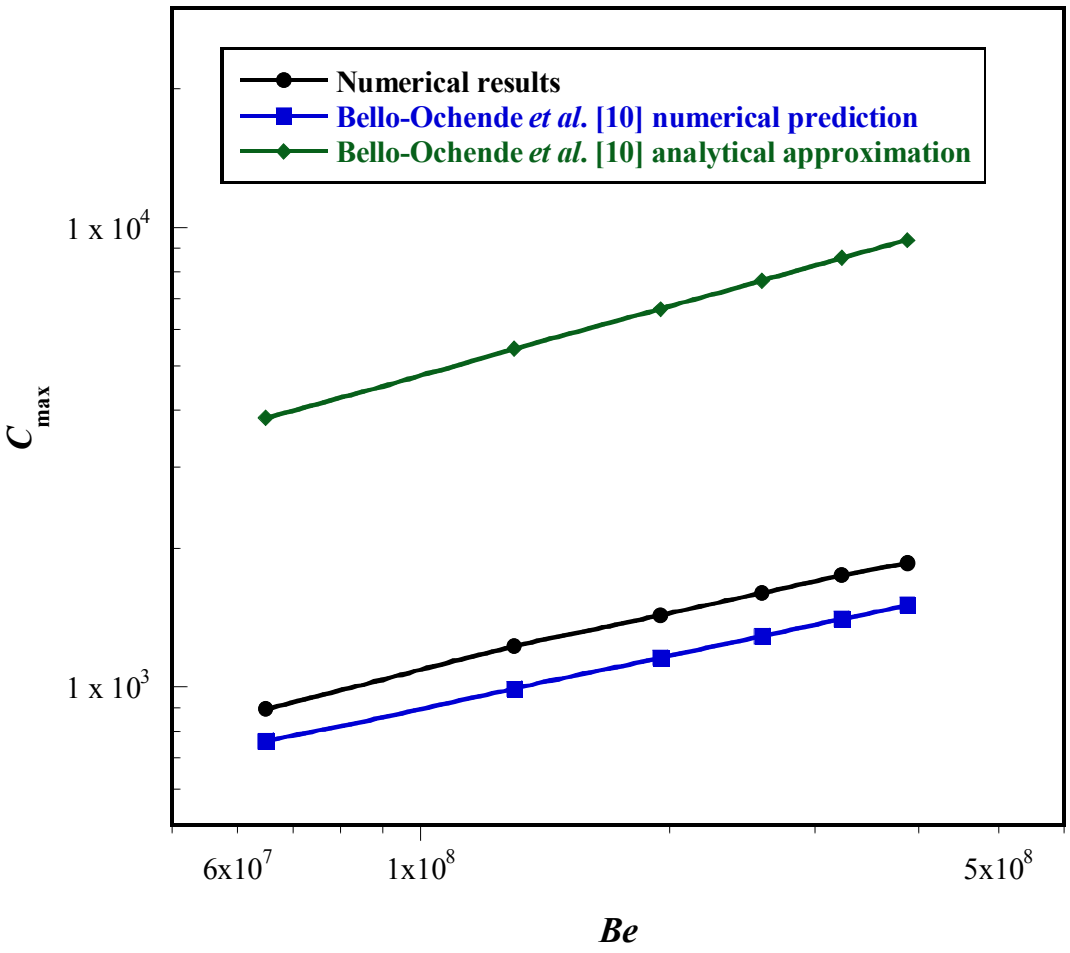

Figure 12. The influence of the dimensionless pressure drop on the maximized global thermal conductance of a heat sink

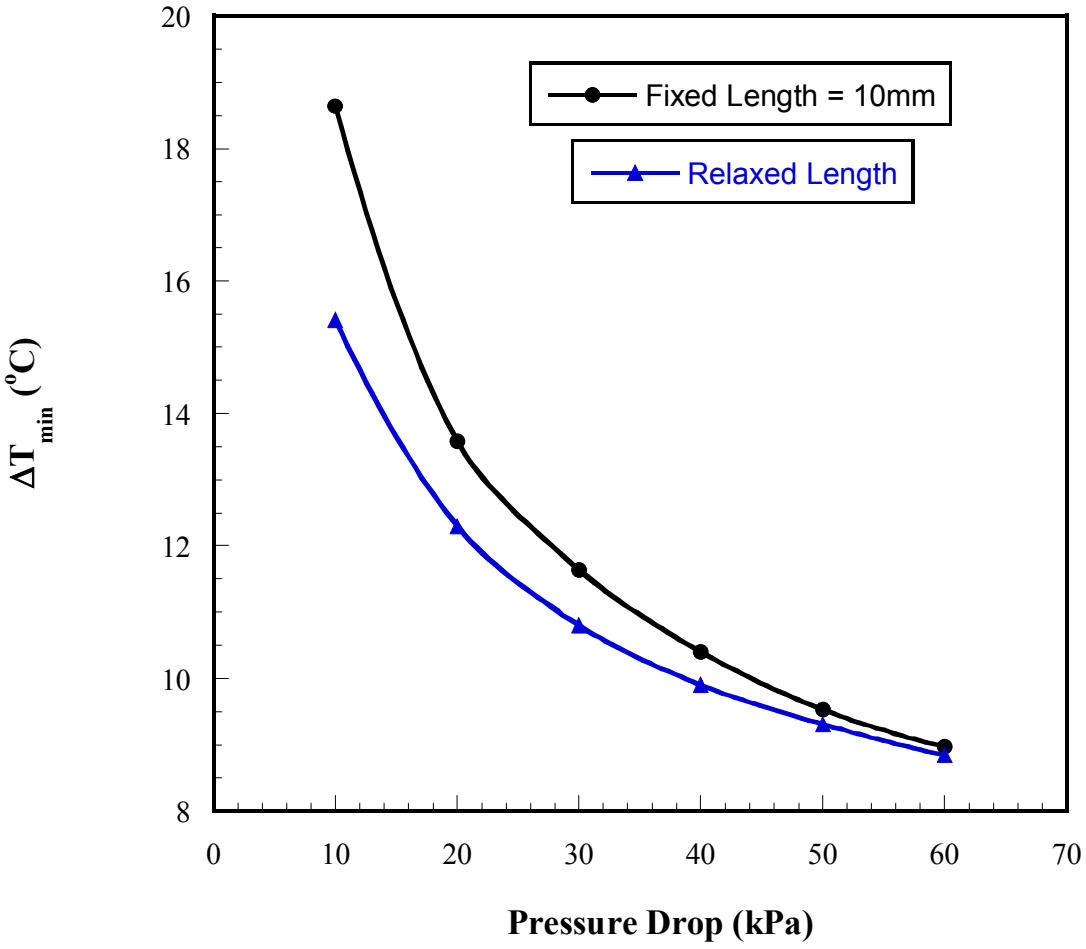

Figure 13. The effect of the relaxation of the axial length as compared to the fixed length optimal peak wall temperature difference

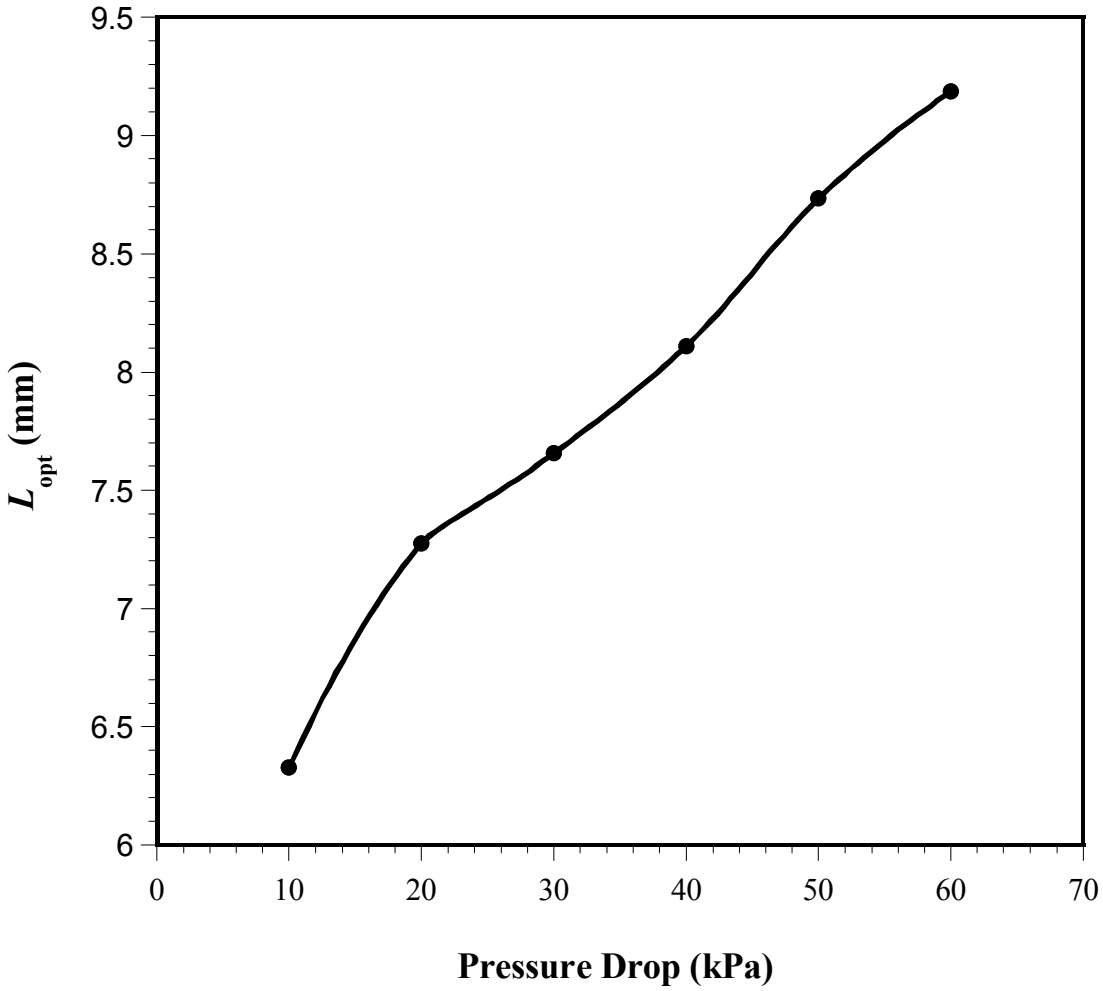

Figure 14. The optimal axial length as a function of the applied pressure drop across the channel

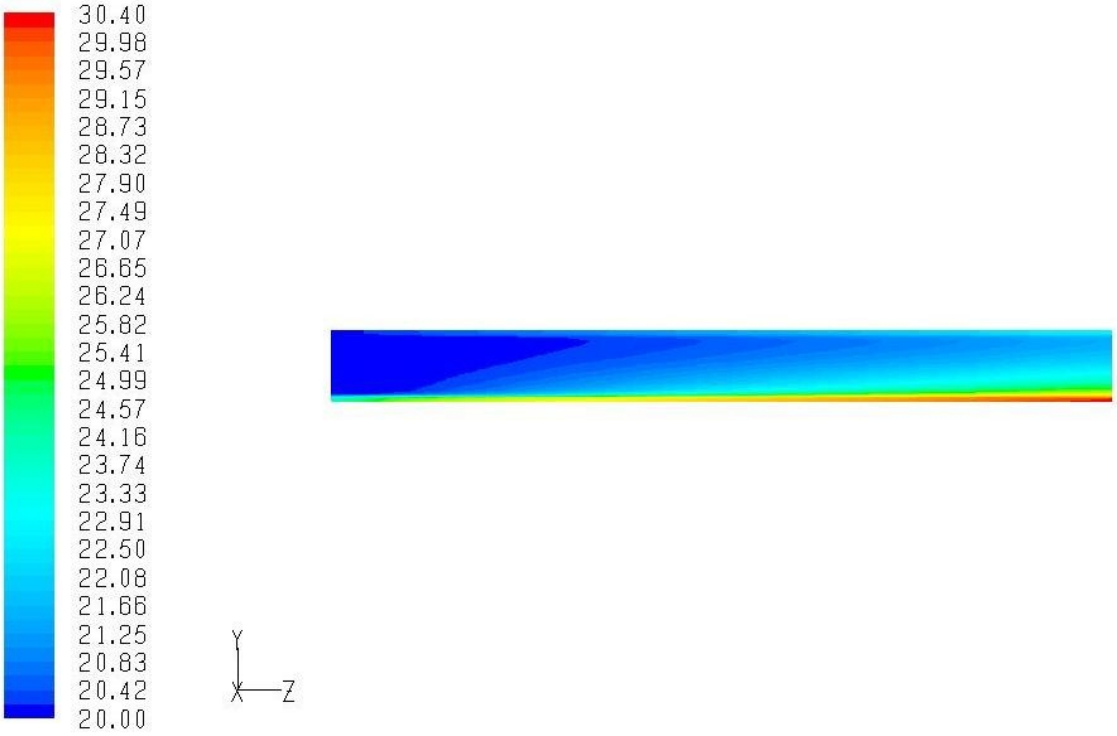

Figure 15a. Temperature distribution (in °C) across the length of the heat sink

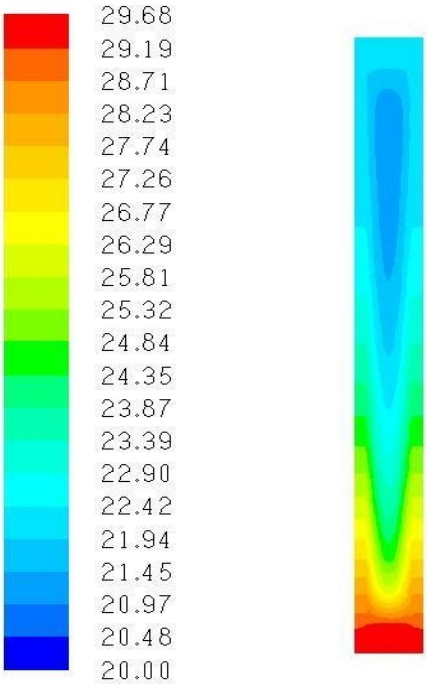

Figure 15b. Temperature distribution (in °C) across the transverse axis of the heat sink

Figure Captions

Figure 1. Physical model of a micro-channel heat sink

Figure 2. Unit cell computational domain for a micro-channel heat sink

Figure 3a. Mesh grid (across the longitudinal axis) generated for numerical computation

Figure 3b. Mesh grid (across the transverse axis) generated for numerical computation

Figure 4. Comparison between numerical and analytical prediction for fully developed velocity profile along the x-axis

Figure 5. Comparison between numerical and analytical prediction for fully developed velocity profile along the y-axis

Figure 6. Comparison between numerical and analytical prediction for Nu profile along the channel length

Figure 7. The optimization process flow chart

Figure 8. The influence of pressure drop on the optimal peak wall temperature difference

Figure 9. The effect of the change in pressure drop on the optimal solid volume fraction

Figure 10. The effect of the change in pressure drop on the optimal channel aspect ratio

Figure 11a. The effect of the change in the pressure drop parameter on the optimal hydraulic diameter

Figure 12. The influence of the dimensionless pressure drop on the maximized global thermal conductance of a heat sink

Figure 13. The effect of the relaxation of the axial length as compared to the fixed length optimal peak wall temperature difference

Figure 14. The optimal axial length as a function of the applied pressure drop across the channel

Figure 15a. Temperature distribution (in °C) across the length of the heat sink

Figure 15b. Temperature distribution (in °C) across the transverse axis of the heat sink